Commun Nonlinear Sci Numer Simulat 149 (2025) 108848

Contents lists available at ScienceDirect

Communications in Nonlinear Science and Numerical Simulation

journal homepage: www.elsevier.com/locate/cnsns

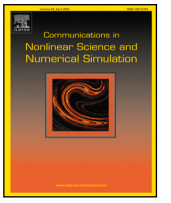

Research paper

Using Lagrangian descriptors to reveal the phase space structure of dynamical systems described by fractional differential equations: Application to the Duffing oscillator

Dylan Theron [a], Hadi Susanto [b], Makrina Agaoglou [c], Charalampos Skokos [a,*]

[a] Nonlinear Dynamics and Chaos Group, Department of Mathematics and Applied Mathematics, University of Cape Town, Rondebosch 7701, South Africa

[b] Department of Mathematics, Khalifa University, PO Box 127788, Abu Dhabi, United Arab Emirates

[c] Departamento de Matemática Aplicada a la Ingeniería Industrial, Escuela Técnica Superior de Ingenieros Industriales, Universidad Politécnica de Madrid, 28006 Madrid, Spain

ARTICLE INFO

Keywords:
Lagrangian descriptors
Fractional differential equations
Duffing Oscillator
Phase space

ABSTRACT

We showcase the utility of the Lagrangian descriptors method in qualitatively understanding the underlying dynamical behavior of dynamical systems governed by fractional-order differential equations. In particular, we use the Lagrangian descriptors method to study the phase space structure of the unforced and undamped Duffing oscillator when fractional-order differential equations govern its time evolution. Our study considers the Riemann–Liouville and the Caputo fractional derivatives. We use the Grünwald–Letnikov derivative, which is an operator represented by an infinite series, truncated suitably to a finite sum as a finite difference approximation of the Riemann–Liouville operator, along with a correction term that approximates the Caputo fractional derivative. While there is no issue with forward-time integrations needed for the evaluation of Lagrangian descriptors, we discuss in detail ways to perform the non-trivial task of backward-time integrations and implement two methods for this purpose: a 'nonlocal implicit inverse' technique and a 'time-reverse inverse' approach. We analyze the differences in the Lagrangian descriptors results due to the two backward-time integration approaches, discuss the physical significance of these differences, and eventually argue that the 'nonlocal implicit inverse' implementation of the Grünwald–Letnikov fractional derivative manages to reveal the phase space structure of fractional-order dynamical systems correctly.

1. Introduction

Fractional calculus, a generalization of classical calculus, extends the concept of derivatives and integrals to non-integer (or fractional) orders. While conventional calculus, attributed to Newton and Leibniz, is well-suited for dealing with integer-order differentials, fractional calculus traces its origins back to Leibniz, who first introduced the concept in a letter to Guillaume de l'Hôpital in 1695, pondering the possibility of a half-order derivative [1]. Unlike classical derivatives, which depend solely on local properties, fractional derivatives account for the history of the function, making them well-suited to model complex systems with memory and hereditary properties, see, e.g., [2–4].

Over the years, fractional derivatives have been successfully used in studies of various physical systems. As examples, we mention

* Corresponding author.
E-mail address: haris.skokos@uct.ac.za (C. Skokos).

https://doi.org/10.1016/j.cnsns.2025.108848
Received 7 January 2025; Received in revised form 30 March 2025; Accepted 5 April 2025
Available online 8 May 2025

the application of fractional derivatives in modeling the viscoelastic behavior of materials, for which traditional integer-order models often fail to capture their time-dependent behavior accurately [5–7]. Fractional derivative models have also been applied to describe the stress–strain relationship in polymers and elastomers, commonly used in various engineering applications, such as vibration dampers and seismic energy dissipation devices. This approach allows for a more accurate representation of the material's response under different loading conditions, including creep, relaxation, and cyclic loading tests [6,8]. Furthermore, a lot of theoretical work has been done on the development of efficient numerical schemes for constructing and computing fractional derivatives and integrals, see, e.g., [9–19]. The dynamics of waves in models with fractional derivatives have also been studied in, e.g., the sine-Gordon equation [20–22].

Despite the increase in utility, providing a physical or geometrical interpretation of fractional integration and differentiation has proven quite tricky. This lack of a suitable interpretation has been discussed in various conferences and meetings, some of which have been mentioned, e.g., in [23]. Since those early conferences, multiple attempts have offered different explanations of fractional calculus. For example, numerous articles have tried to link fractional calculus and fractal geometry (see, e.g., [24–26]). Additional examples of explanatory attempts include providing an interpretation of a fractional order Grünwald–Letnikov differintegral by measuring the path and acceleration of a point in motion [27], or by first offering a straightforward geometric elucidation of fractional integrals, which is then used to introduce a physical understanding of the Riemann–Liouville fractional integration with respect to a dynamic time scale [23]. Quoting Podlubny (2001), "...it is difficult to speak about an acceptable geometric interpretation if one cannot see any picture there" [23]. In this work, we offer an approach of qualitatively visualizing phase space structures of dynamical systems governed by fractional differential equations through implementing the Lagrangian descriptors method [28]. Our work is, therefore, expected to pave the way toward providing a physical and geometrical interpretation of fractional derivatives.

The Lagrangian descriptors method is a tool that helps to identify phase space structures of systems governed by integer-order differential equations, including invariant manifolds [29]. These descriptors are scalar functions obtained by the time integration of a positive quantity, such as the modulus of velocity or acceleration, along particle trajectories over a finite time interval. By evaluating these quantities through the evolution of trajectories, both forward and backward in time, one can provide a comprehensive picture of the underlying dynamics in a computationally efficient way compared to traditional methods, like the computation of finite-time Lyapunov exponents [30]. The method of Lagrangian descriptors was first introduced in [31] and was initially inspired by efforts to explain the geometric patterns that control transport in geophysical flows. Since then, Lagrangian descriptors have found various applications in fields such as chemical reaction dynamics [28,32–37], geophysical flows [31,38–42], cardiovascular flows [43], biomedical flows [44], and billiard dynamics [45], to name a few. In addition, Lagrangian descriptors have also been used as diagnostics of chaotic behavior [29,46–48]. As a more general remark, we note that approaches based on the Lagrangian description of dynamical systems have been used to study phase space structures in diverse research fields ranging from plasma physics to oceanic flows [49–53].

In this paper, we apply the method of Lagrangian descriptors for the first time to systems governed by fractional-order differential equations to obtain their phase portraits, which would not be possible using traditional methods due to the nonlocal character of fractional-order differential equations. It is worth mentioning that this nonlocality creates difficulties in calculating the backward-in-time part of the Lagrangian descriptors, a topic that we also address in this work.

The paper is organized as follows. In Section 2, we present the definitions of the various fractional time derivatives used in this paper, while in Section 3, we present the Lagrangian descriptors method. Then, in Section 4, we use Lagrangian descriptors computations to visualize the phase space structure of the Duffing oscillator when its dynamics are described by fractional-order differential equations and present different approaches of performing backward time integrations. In addition, we discuss in detail which of these approaches manage to reveal the phase space structure of the system correctly. In Section 5, we present our conclusions and discuss potential future work directions.

2. Fractional derivatives

Unlike classical integer-order derivatives, fractional derivatives offer a more flexible framework that arises from how fractional calculus can be generalized from its classical counterpart. The concept of fractional differentiation is, therefore, not unique, and over the years, numerous definitions of fractional derivatives have been proposed [54]. The most well-known definitions include the Riemann–Liouville fractional derivative, the Caputo derivative, and the Grünwald–Letnikov derivative. Each of these definitions is based on distinct mathematical principles, yet they aim to extend the concept of differentiation to non-integer orders, e.g., [55].

The Riemann–Liouville fractional derivative is among the oldest and most widely used definitions. It is based on an integral operator and offers a natural extension of integer-order differentiation. Let $C^n(I,\mathbb{R})$ denote the space of n-times continuously differentiable single variable real-valued functions on the real interval I. We also let $\alpha \in (0,\infty)\setminus\mathbb{N}$ and the function $g \in C^n([a,b],\mathbb{R})$. The (left-sided) Riemann–Liouville fractional-order derivative of order α of the function g at point t is given by

$$ {}^{RL}D^{\alpha}_{a+}g(t) = \frac{1}{\Gamma(n-\alpha)}\frac{d^n}{dt^n}\int_a^t (t-s)^{n-\alpha-1}g(s)ds, \tag{1}$$

where $n = \lfloor\alpha\rfloor+1$ and $\Gamma(x)$ is the usual Gamma function. This fractional derivative can be defined for absolutely continuous functions of order n, i.e., $g \in AC^n([a,b],\mathbb{R})$, which does not necessarily require the existence of the n-th derivative of the function. This is highlighted in Lemma 2.2 on page 73 of [2]. This less strict requirement is sufficient, particularly since our analysis is restricted to the case $0 < \alpha < 1$. However, the assumption of C^n smoothness is commonly made for simplicity.

The definition of fractional derivatives (1) presents challenges in practical applications for the following reasons. In initial value problems with classical (integer-order) differential equations, initial conditions typically specify the function's values and integer-order derivatives at a given point. However, initial value problems with non-integer order Riemann–Liouville derivatives often require initial conditions involving integrals or fractional integrals of the function [2,56,57]. As a result, standard initial conditions (i.e., specifying the value of the function at a single point) may not be sufficient, and one might need to specify additional conditions based on past behavior. This requirement adds complexity to solving fractional initial value problems with the Riemann–Liouville definition. In that scenario, interpreting and applying this type of fractional derivatives in real-world scenarios where initial values are typically simple, such as initial positions or velocities in mechanical systems, becomes challenging.

Caputo modified the classical Riemann–Liouville fractional derivative to address the practical issues related to the initial conditions. The primary motivation behind Caputo's formulation was to make fractional derivatives more suitable for modeling physical processes, i.e., initial value problems, particularly in applications where classical initial conditions (such as those used in integer-order differential equations) are commonly used. The (left-sided) Caputo fractional-order derivative of order α of a function g is given by

$$ {}^{C}D^{\alpha}_{a+}g(t) = \frac{1}{\Gamma(n-\alpha)}\int_a^t (t-s)^{n-\alpha-1}\frac{d^n g(s)}{ds^n}ds. \tag{2} $$

The Caputo derivative can be written in terms of the Riemann–Liouville derivative as follows

$$ {}^{RL}D^{\alpha}g(t) = {}^{C}D^{\alpha}g(t) + \sum_{k=0}^{n-1}\frac{g^{(k)}(0^+)}{\Gamma(k-\alpha+1)}t^{k-\alpha}. \tag{3} $$

These two fractional derivatives coincide when the initial conditions are zero (homogeneous), i.e., $g^{(k)}(0^+) = 0$, $k = 0, \dots, n-1$, see e.g., [58]. While the Caputo derivative is often preferred in modeling physical systems, the Riemann–Liouville derivative is favored for its historical significance and analytical tractability.

Grünwald and Letnikov generalized the notion of finite differences to non-integer orders. They worked on extending the concept of differentiation and integration to fractional orders using finite differences, naturally leading to a discretized form of fractional derivatives. The Grünwald–Letnikov fractional derivative of order α of function g is given by

$$ {}^{GL}D^{\alpha}_{a+}g(t) = \lim_{h\to 0} h^{-\alpha}\sum_{r=0}^{[(t-a)/h]}(-1)^r\binom{\alpha}{r}g(t-rh), \tag{4} $$

where the generalized binomial coefficient is

$$ \binom{\alpha}{k} = \frac{\alpha(\alpha-1)(\alpha-2)\dots(\alpha-k+1)}{k!} = \frac{\Gamma(\alpha+1)}{\Gamma(k+1)\Gamma(\alpha-k+1)}. $$

It is important to note that if $\alpha \in (0,\infty)\setminus\mathbb{N}$ and $g : (0,\infty)\to\mathbb{R}$ is a function of class C^n, then [2,56]

$$ {}^{RL}D^{\alpha}g(t) = {}^{GL}D^{\alpha}g(t). \tag{5} $$

The Grünwald–Letnikov derivative (4), therefore, provides a framework for the numerical computation of the Riemann–Liouville fractional derivative. However, since the Riemann–Liouville derivative was formally introduced slightly later, Grünwald and Letnikov did not set their work explicitly as its discretization. Using (3), we can also obtain the Grünwald–Letnikov representation for the Caputo derivative [58]. We consider the Riemann–Liouville and Caputo derivatives using their Grünwald–Letnikov representations in this work.

3. Lagrangian descriptors

The Lagrangian descriptors method involves summing, for any initial condition of a dynamical system, the values of a positive scalar function that depends on phase space variables along its trajectory, both forward and backward in time. This process is applied to a grid of initial conditions on a specific phase space slice to uncover the underlying dynamical structure. Furthermore, in the case of dynamical systems described by integer-order differential equations or of discrete-time systems, the resulting scalar field of Lagrangian descriptors highlights invariant stable and unstable manifolds, which appear as 'singular features' where the descriptor values change abruptly. Forward trajectory integration identifies stable manifolds, while backward trajectory evolution identifies unstable manifolds. In this paper, we use the following pseudonorm-like scalar functional as the Lagrangian descriptor [59]

$$ M_p(\mathbf{x}_0,t_0,\tau) = M_p^b(\mathbf{x}_0,t_0,\tau) + M_p^f(\mathbf{x}_0,t_0,\tau), \tag{6} $$

where

$$ M_p^b(\mathbf{x}_0,t_0,\tau) = \int_{t_0-\tau}^{t_0}\sum_{i=1}^{N}\left|f_i(\mathbf{x},t)\right|^p dt, \quad M_p^f(\mathbf{x}_0,t_0,\tau) = \int_{t_0}^{t_0+\tau}\sum_{i=1}^{N}\left|f_i(\mathbf{x},t)\right|^p dt, \tag{7} $$

with $f_i(\mathbf{x},t)$ being the ith component of a vector field, while t_0 is the time at which we start the evolution of the studied trajectory (in this study we set $t_0 = 0$), τ is the integration time, and $\mathbf{x}_0$ is the initial condition of the considered orbit. The superscripts f and b indicate the forward- and backward-in-time Lagrangian descriptors method. The functional (6) resembles a p-norm, but with

$p \in \mathbb{R}$. We select the parameter p to allow for the greatest discontinuity of the gradient of the Lagrangian descriptor values at the manifold, thus permitting us to extract the normally hyperbolic invariant manifolds (NHIMs) [60] from the Lagrangian descriptors scalar field. It has been shown that this occurs at $p = 1/2$ for a wide variety of dynamical systems [61,62].

The formulation (6) has been used for dynamical systems governed by ordinary differential equations. Our model is governed by fractional-order differential equations that we solve as a discrete-time dynamical system. For this reason, we define the discrete Lagrangian descriptors in the following pseudonorm form (see, e.g., [29,35,63])

$$MD_p(\mathbf{x_0}, N) = MD_p^-(\mathbf{x_0}, N) + MD_p^+(\mathbf{x_0}, N), \tag{8}$$

where

$$MD_p^-(\mathbf{x_0}, N) = h^{1-p} \sum_{j=-N}^{-1} \sum_{i=1}^{k} |x_{j+1}^i - x_j^i|^p, \quad MD_p^+(\mathbf{x_0}, N) = h^{1-p} \sum_{j=0}^{N-1} \sum_{i=1}^{k} |x_{j+1}^i - x_j^i|^p \tag{9}$$

respectively are the backward and forward evolution of the orbit with initial condition $\mathbf{x_0}$. Furthermore, x_j^i represents the ith component of the state vector $\mathbf{x}$ at time t_j and $h = (t_{j+1} - t_j) \ll 1$ is the discretization time step.

4. Numerical results

To illustrate the application of the Lagrangian descriptors method for revealing the phase portrait of dynamical systems with fractional derivatives, we consider the unforced and undamped Duffing oscillator governed by fractional-order differential equations:

$$\begin{aligned} D^\alpha x(t) &= y(t), \\ D^\alpha y(t) &= x(t) - x(t)^3, \end{aligned} \tag{10}$$

where D^α denotes the fractional derivative of order α. When $\alpha = 1$, system (10) reduces to the classical Duffing oscillator originally described in [64]. For non-integer values of α, the system represents a fractional Duffing oscillator in which the concept of acceleration is generalized, where the system's present state depends not only on current values but also on its entire past trajectory. This reflects the memory effect inherent to fractional calculus.

The fractional derivative can be viewed as a continuous interpolation between integer-order derivatives. For instance, considering an alternative fractional-order Duffing oscillator as $D^{2\alpha}x(t) = x(t) - x(t)^3$ with $0.5 < \alpha < 1$, the derivative lies between the first derivative (velocity) and the second derivative (acceleration), thereby capturing intermediate dynamical behavior. Variants of the Duffing oscillator incorporating damping and external forcing in the fractional-order setting have been studied in, e.g., [65–67], with a focus on chaotic dynamics, bifurcation structures, and the emergence of multistability induced by fractional effects. An alternative approach to introducing fractionality is through the damping term rather than the acceleration, allowing for the modeling of complex energy dissipation mechanisms. This has been explored in works such as [68–73], where the memory-dependent dissipation leads to rich dynamics, including slow energy decay and long-term memory effects.

In this study, however, our objective is to demonstrate the effectiveness of the Lagrangian descriptors method in analyzing dynamical systems with fractional derivatives. To this end, we focus on the simplest form of the fractional Duffing oscillator (10), omitting damping and external forcing to isolate and examine the impact of fractionality alone. Note that the fractional equations, for all the different fractional derivatives used, exhibit invariance under the transformation $x \to -x$ and $y \to -y$. This symmetry, referred to as "point symmetry", implies that the solutions of the system are symmetric with respect to the origin. Consequently, we expect the phase space structures and results presented in this work will display this symmetry. Its presence in our results will confirm that the numerical simulations are consistent and reasonable.

4.1. Phase space structures

The Lagrangian descriptors method has been successfully applied to the classical Duffing oscillator (10) with $\alpha = 1$ [28], as well as to variants such as stochastic Duffing systems [74]. This method yields a scalar field highlighting key geometric structures in the phase space, including saddle points, attractors, repellers, and NHIMs. By integrating trajectories over a finite time interval, the Lagrangian descriptors method enables efficient visualization of these structures without requiring long-time simulations. To perform backward-in-time integration for dynamical systems described by integer-order derivatives, we can reverse the direction of the time variable and integrate the dynamical system by using the same numerical methods but with negative time steps.

In Fig. 1, we present results for the classical Duffing oscillator using the pseudonorm definition of Lagrangian descriptors (6). The computations were performed over a grid of 1000×1000 equidistant initial conditions in the domain $x \in [-1.5, 1.5]$ and $y \in [-1, 1]$, for integration times $\tau = 5$ [Fig. 1(a)] and $\tau = 10$ [Fig. 1(b)]. The color bars indicate the magnitude of the Lagrangian descriptor values in each panel. From these results, three fixed points are identifiable: two stable equilibria at $(x, y) = (\pm 1, 0)$, and one unstable saddle at the origin $(x, y) = (0, 0)$. By using linearization, one finds that the equilibria at $(x, y) = (\pm 1, 0)$ have purely imaginary eigenvalues $\lambda = \pm\sqrt{2}i$, indicating centers in the linearized system. In contrast, the origin has real eigenvalues $\lambda = \pm 1$, characterizing it as a saddle point. The stable and unstable manifolds of the origin connect to form an "infinity-shaped" separatrix structure. Additionally, low Lagrangian descriptor values are observed near the stable equilibria, corresponding to regions of slower dynamical variation. Normally hyperbolic invariant manifolds appear as sharply defined curves in the Lagrangian descriptor scalar field, characterized by strong gradient transitions in the descriptor values [34]. Their nearly identical appearance across both panels

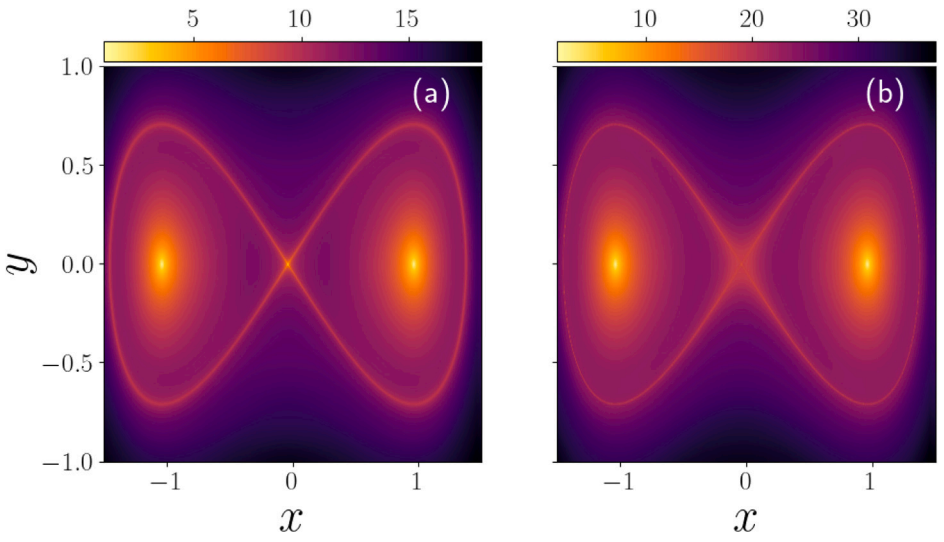

Fig. 1. Initial conditions colored according to their Lagrangian descriptor value (6), by using the color bar above each panel of the classical Duffing oscillator, i.e., system (10) for $\alpha = 1$. The two panels are constructed for a grid of 1000×1000 equidistant initial conditions over the intervals $x \in [-1.5, 1.5]$ and $y \in [-1, 1]$ and show results for an integration time of (a) $\tau = 5$ and (b) $\tau = 10$.

in Fig. 1 reflects their invariant nature, as discussed in [60]. As expected, the overall magnitude of the Lagrangian descriptor values increases with the integration time, from $\tau = 5$ to $\tau = 10$, due to the cumulative nature of the computation.

Since the dependence of the model on the fractional order α is continuous, the behavior of the system governed by fractional-order derivatives smoothly converges to that of its integer-order counterpart as α approaches an integer. In particular, the fractional derivative operator and the corresponding solutions tend to their classical analogs. Consequently, the phase space structures of the fractional model converge to those of the integer-order system. The results in Fig. 1, corresponding to the integer-order case $\alpha = 1$, will therefore serve as a reference for analyzing how the phase space structures evolve under fractional-order dynamics with $0 < \alpha < 1$.

In the context of fractional-order dynamical systems with derivative orders $\alpha \leq 1$, the definition of phase space requires clarification. Unlike integer-order systems, where the phase space dimension corresponds directly to the number of initial conditions needed to uniquely specify a solution, fractional-order dynamical systems exhibit memory effects that complicate this correspondence. Nevertheless, since our analysis is restricted to the initial value problem with fixed starting time $t = 0$ and fractional derivatives of order $\alpha \leq 1$, the solutions depend uniquely on the finite set of initial values $x(0)$ and $y(0)$. Therefore, we define an effective two-dimensional phase space, reflecting the minimal data required to initiate a solution at $t = 0$ uniquely. We note, however, that if the problem were to be re-initialized at a later time $t_0 > 0$ with a fixed lower limit of integration at 0 [see Eqs. (1) and (2) with $a = 0$], an infinite history would be required.

The challenge in calculating Lagrangian descriptors for fractional derivatives lies in the backward integration of the equations of motion (10), as required by the method [see Eq. (7)]. This inverse time integration involves solving the differential equations by stepping backward along the time axis, effectively reversing the system's time evolution. While this approach is useful in applications such as reconstructing past states from current data or performing sensitivity analysis, it introduces numerical stability challenges. Specifically, many physical systems governed by dissipative processes are inherently irreversible, meaning small numerical errors during backward integration can accumulate exponentially, leading to inaccurate or non-physical solutions. In this work, we consider two approaches for solving the backward-in-time integration.

The first approach follows the integer-order system, where we apply the transformation $t \to -t$. In this case, the backward dynamics of the Duffing oscillator are derived from (10) as follows:

$$\begin{aligned} D^{\alpha} x(t) &= -y(t), \\ D^{\alpha} y(t) &= -x(t) + x(t)^3, \end{aligned} \tag{11}$$

which can be evolved using the same one-step method applied to (10) (e.g., the Grünwald–Letnikov or Caputo derivative). We refer to this method as the 'time-reversing inverse' approach. However, in the case of fractional-order derivatives, Eq. (11) no longer provides the correct backward trajectory of the system [75]. This is due to the intrinsic memory property of fractional derivatives, where the evolution of the system depends not only on its current state but also on its entire history. We therefore consider the following second approach, which is more complex, as reconstructing past states requires knowledge of the entire trajectory rather than just a finite set of current values.

To determine the initial state $\mathbf{x} = \mathbf{x_0}$ at time $t = 0$ from a given future state $\mathbf{x_N}$ at $t = t_N$, we must solve equations that depend on all unknown past values of the state vector $\mathbf{x}$ between $t = 0$ and $t = t_N$. Therefore, the backward time integration method

becomes implicit for the Grünwald–Letnikov derivative (4). In this case, we must simultaneously solve a set of algebraic nonlinear equations for all time steps, which we do using the Newton–Raphson method. We call this approach the 'nonlocal implicit inverse' method. However, when implementing this method, we found that numerical convergence was not always achieved for certain initial conditions. This issue became more pronounced when using the Caputo version of the fractional derivative (2) with the 'nonlocal implicit inverse' method. For the sake of comparison, we therefore use (11) for the Caputo derivatives with fractional α.

We now apply the Lagrangian descriptors method (6) to analyze the phase space structures of the Duffing oscillator governed by fractional-order differential Eqs. (10). The results are presented in Fig. 2, for various integration times τ and fractional orders α. To facilitate direct comparison with the results obtained for $\alpha = 1$ (Fig. 1), all panels in Fig. 2 were generated using a grid of 100×100 equidistant initial conditions over the same interval considered in Fig. 1. We emphasize that a sparser grid was used instead of the 1000×1000 grid points employed in Fig. 1 due to the significantly higher computational costs associated with integrating fractional differential equations.

The results obtained using the 'nonlocal implicit inverse' method with the Grünwald–Letnikov fractional derivative are presented in the first column of Fig. 2 for an integration time of $\tau = 5$. The remaining panels in the second and third columns of Fig. 2 display the Lagrangian descriptor values computed using the 'time-reversing inverse' method with the Caputo derivative. The results in the second and third columns correspond to an integration time of $\tau = 5$ and $\tau = 10$, respectively. Note that the 'nonlocal implicit inverse' method was only applied in the first column for an integration time of $\tau = 5$, as this approach requires significantly higher computational resources than the 'time-reversing inverse' method used in the second and third columns.

Each row of plots in Fig. 2 illustrates the phase space structures of the Duffing oscillator described by (10) for different fractional orders α. We observe similar infinity-shaped phase space structures in all panels of the top row. This similarity suggests that for $\alpha = 0.9999$ – a value very close to the integer-order case ($\alpha = 1$) – the formations revealed by the Lagrangian descriptors method are approximately invariant to both the chosen integration time τ and the fractional derivative method employed. Furthermore, the nearly identical shapes of the phase space patterns in Fig. 2(a)–(c) closely resemble those observed in Fig. 1. We also note that the ranges of Lagrangian descriptor values (indicated by the color bars above each panel in Fig. 2) are approximately equivalent to those seen in the corresponding panels of Fig. 1 for the same integration time τ.

Reducing the fractional order of the dynamical system slightly to $\alpha = 0.99$ for the 'nonlocal implicit inverse' method [Fig. 2(d)] results in an infinity-shaped structure that is no longer continuous and connected. Instead, the structure exhibits breaks at both edges of the x-axis. Notably, the phase portrait in Fig. 2(d) exhibits point symmetry about the origin. In the plots obtained using the 'time-reversing inverse' method [Fig. 2(e), (f)], the structures revealed by the Lagrangian descriptors method demonstrate a clear dependence on the integration time τ. For $\tau = 5$ [Fig. 2(e)], the phase space formations closely resemble those observed for $\alpha = 0.9999$ with the same integration time [Fig. 2(b)]. Increasing the integration time to $\tau = 10$ [Fig. 2(f)] reveals an additional curve outside the infinity-shaped feature. It is worth noting that the structures generated by the 'time-reversing inverse' approach in Fig. 2(e), (f) exhibit reflective symmetry with respect to the horizontal and vertical axes passing through the origin $(x, y) = (0, 0)$. Further decreasing the fractional derivative order to $\alpha = 0.98$ leads to an infinity-like structure with more pronounced breaks when the 'nonlocal implicit inverse' approach is used [Fig. 2(g)]. In the results obtained using the 'time-reversing inverse' methods [Fig. 2(h), (i)], we observe geometric patterns similar to those presented in Fig. 2(e), (f) for $\alpha = 0.99$. However, for $\tau = 10$ [Fig. 2(i)], the distances between the additional curves increase compared to those observed in Fig. 2(f).

From the results presented in Fig. 2, we observe that for $\alpha \approx 1$, the phase space structures closely resemble those of the integer-order ($\alpha = 1$) Duffing oscillator analyzed in Fig. 1. These structures are practically unaffected by the specific realization of the fractional derivatives or the integration time τ. However, as the fractional order of the dynamical system is slightly reduced (while remaining close to $\alpha = 1$), the phase space geometries revealed by the Lagrangian descriptors exhibit dependence on both the integration time τ and the particular methods used to evaluate the backward-in-time fractional derivatives. To illustrate how the phase space features evolve as the fractional order α is further decreased, we present in Fig. 3 phase space plots analogous to those in Fig. 2, but for $\alpha = 0.95$ [Fig. 3(a)–(d)] and $\alpha = 0.9$ [Fig. 3(e)–(h)].

Fig. 3(a) and (d) present results obtained using the 'nonlocal implicit inverse' method. Several points in these plots are colored white, indicating initial conditions for which the backward-in-time evolution could not be computed due to the non-convergence of the implemented root-finding method. Additionally, as the fractional order of the system decreases from $\alpha = 0.95$ [Fig. 3(a)] to $\alpha = 0.9$ [Fig. 3(d)], we observe an increase in the number of these white points. This trend suggests that the 'nonlocal implicit inverse' method is approaching the limits of its applicability and cannot be efficiently used for smaller α values. In contrast, the 'time-reversing inverse' approach, used to generate the results in the right two columns of Fig. 3, remains applicable even for smaller α values. The phase space patterns in Fig. 3(a) and (d) show a substantial break of the branches that previously formed the well-defined infinity-shaped structure. This disconnection becomes more pronounced as α decreases, leading to phase space patterns that differ significantly from those observed in the integer-order case presented in Fig. 1. Despite these changes, the point symmetry of the structures – previously observed in Fig. 2(a), (d), and (g) – is still preserved.

The results obtained using the Caputo derivative with the 'time-reversing inverse' approach are presented in Fig. 3(b), (c) for $\alpha = 0.95$ and in Fig. 3(e), (f) for $\alpha = 0.9$. We note that the phase portraits in all these figures retain reflective symmetry with respect to the horizontal and vertical axes passing through the origin, consistent with the observations in the right two columns of Fig. 2. For both $\alpha = 0.95$ and $\alpha = 0.9$, the infinity-shaped structure remains well-defined for $\tau = 5$ [Fig. 3(b) and (e)]. For $\tau = 10$ and $\alpha = 0.95$ [Fig. 3(c)], an additional curve appears outside the infinity-shaped formation, similar to the patterns observed in Fig. 2(f) and (i). However, the distance between these two structures is larger than those observed in Fig. 2(f) and (i). As the integration time increases [from Fig. 3(e) to Fig. 3(f)], the color of the curves becomes darker, indicating changes in the Lagrangian descriptor values.

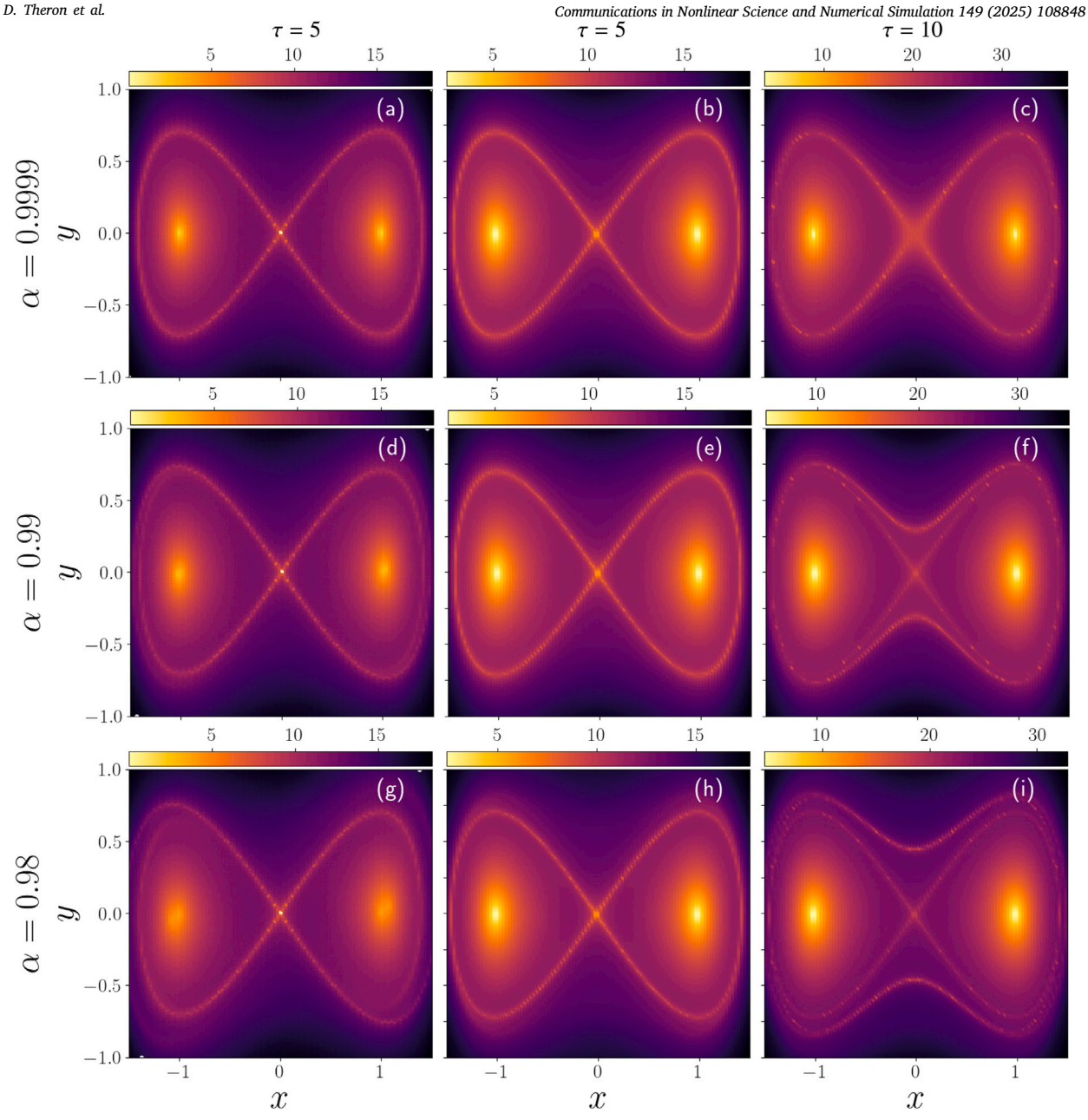

Fig. 2. The phase space of the Duffing oscillator governed by the fractional differential Eqs. (10) is presented for various fractional orders α (indicated on the left of each row) and integration times τ (indicated at the top of each column). Each initial condition is colored according to its Lagrangian descriptor value, as shown by the color bar above each panel. The plots are generated using a grid of 100×100 equidistant initial conditions over the intervals $x \in [-1.5, 1.5]$ and $y \in [-1, 1]$. The first column of results [panels (a), (d), and (g)] reveals the phase space structure obtained using the Grünwald–Letnikov method (4), following the 'nonlocal implicit inverse' approach (see the main text for details). The remaining panels in the second and third columns correspond to results obtained using the Caputo derivative with the 'time-reversing inverse' method.

Using the 'time-reversing inverse' method, the Lagrangian descriptors can still be computed for smaller α values. However, as previously noted, this is not feasible with the 'nonlocal implicit inverse' approach, which has reached its practical limits for smaller α values.

4.2. Which method reveals the correct dynamical behavior?

Having computed the Lagrangian descriptors of the Duffing oscillator governed by fractional differential equations (10) using two different backward-time integration methods, we observe from Figs. 2 and 3 that these methods yield qualitatively different results.

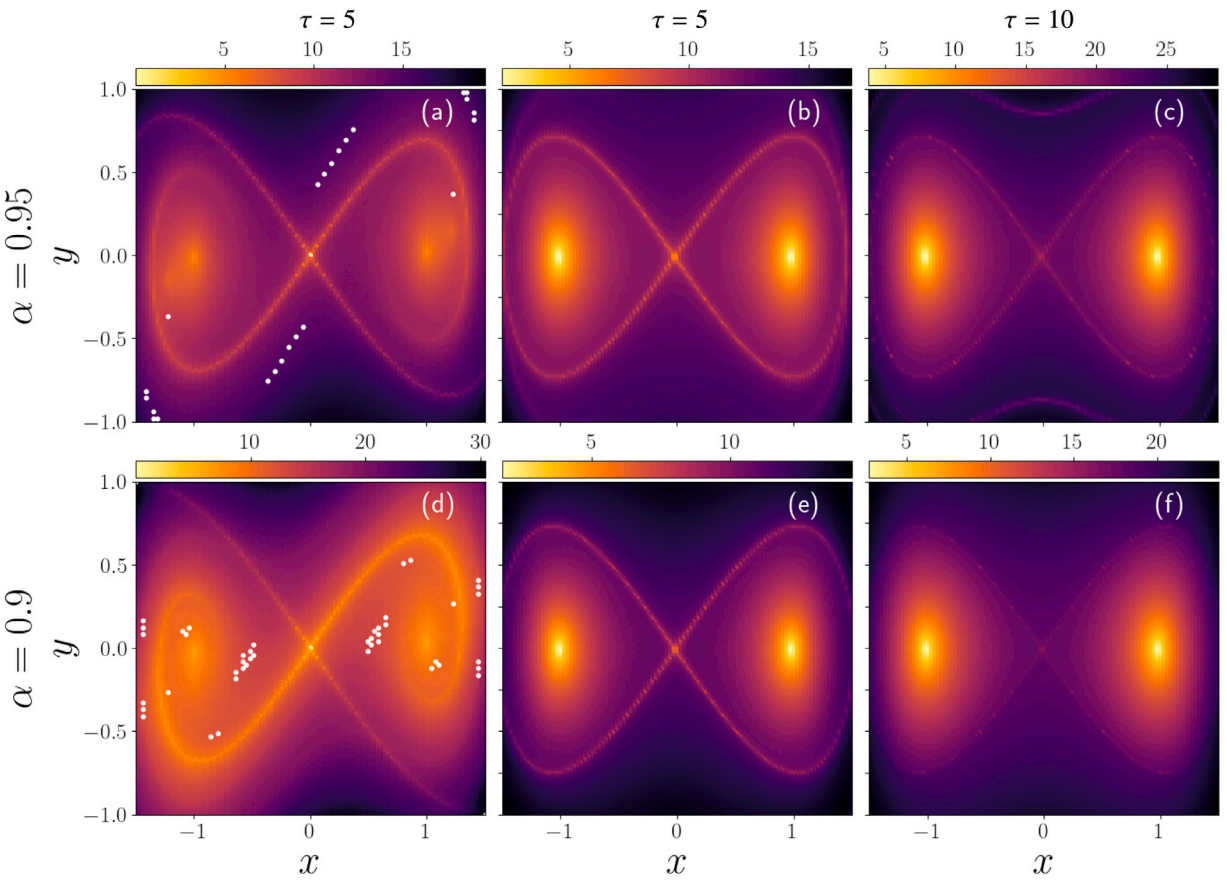

Fig. 3. Plots similar to those seen in Fig. 2, but for $\alpha = 0.95$ [first row, panels (a)–(c)] and $\alpha = 0.9$ [second row, panels (d)–(f)]. White-colored points in panels (a) and (d) correspond to initial conditions whose backward time evolution was not computed due to the numerical instabilities of the implemented algorithm.

In particular, one method results in broken NHIMs, while the other preserves their smoothness and continuity. These differences arise directly from the distinct backward integration schemes employed. This naturally raises the question: which method provides Lagrangian descriptors that accurately represent the phase space structure of the fractional-order dynamical system?

To address this question, we first revisit the notion of equilibrium solutions in fractional-order systems. The equilibrium points of systems with the Caputo derivative coincide with those of the corresponding integer-order system; see, e.g., [76] and references therein. The linear asymptotic stability of an equilibrium is determined by the condition $|\arg(\lambda)| > \alpha\pi/2$, where λ denotes the eigenvalues of the linearized system [77–79]. If this condition is not satisfied, the equilibrium is linearly unstable. Using this result, the equilibria $(x, y) = (\pm 1, 0)$ of the system (10) with the Caputo derivative will become asymptotically stable for $0 < \alpha < 1$, while the origin $(x, y) = (0, 0)$ remains unstable.

On the other hand, fractional systems involving the Riemann–Liouville derivative generally do not admit standard time-independent equilibria [76]. This is because, as seen directly from (1), the Riemann–Liouville derivative of a non-trivial constant does not vanish. Specifically, for $0 < \alpha < 1$, we have

$$ {}^{RL}D^{\alpha}_{0+} 1 = \frac{t^{-\alpha}}{\Gamma(1-\alpha)}. $$

Therefore, only the trivial constant solution – when it corresponds to an equilibrium in the associated integer-order system – can persist as an equilibrium in the Riemann–Liouville framework. Its stability is determined by the same criterion as in the Caputo case [80]. Consequently, the origin $(x, y) = (0, 0)$ remains a saddle point of the system (10). In contrast, the nontrivial equilibria $(x, y) = (\pm 1, 0)$, which exist when $\alpha \in \mathbb{N}$, no longer qualify as true equilibria for $0 < \alpha < 1$. We refer to them as *quasi-equilibria* since the dynamics of the system tend toward these points in the limit $t \to \infty$, as we will show below.

Next, we turn our attention to the Duffing oscillator with $\alpha = 0.95$, focusing on the phase portraits generated using the Riemann–Liouville and Caputo fractional derivatives, computed with the 'nonlocal implicit inverse' and 'time-reversing inverse' methods, respectively, for an integration time of $\tau = 5$ [Fig. 3(a) and (b)]. In these cases, we analyze the relationship between the phase space patterns obtained from the forward and backward Lagrangian descriptors (7) and the corresponding forward and backward time evolution of selected trajectories. The results of this comparison are presented in Fig. 4.

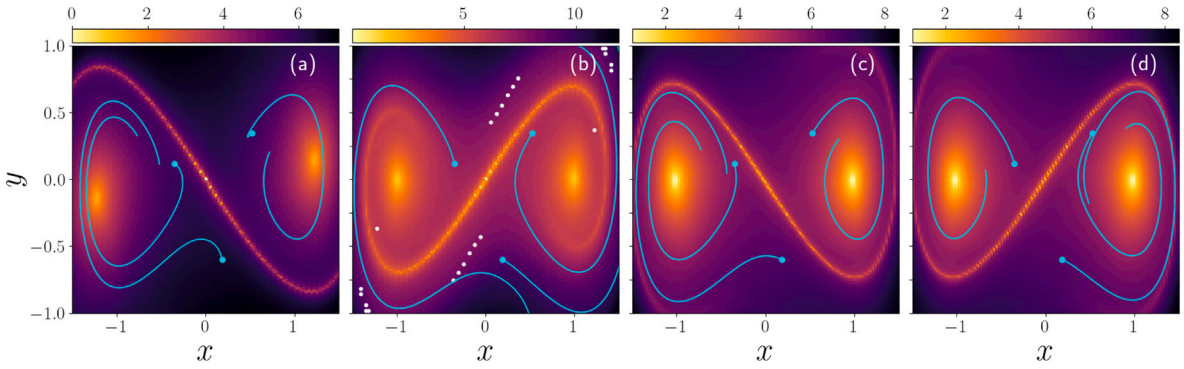

Fig. 4. Initial conditions of the Duffing oscillator governed by the fractional differential Eqs. (10) with $\alpha = 0.95$, colored according to their Lagrangian descriptor values (using the color scale shown above each panel). The plots are generated using an equidistant grid of 100×100 points over the intervals $x \in [-1.5, 1.5]$ and $y \in [-1, 1]$, with an integration time of $\tau = 5$. The Grünwald–Letnikov derivative (4) is used for the forward-time evolution of orbits to generate panel (a), and its 'nonlocal implicit inverse' version is applied in panel (b) for the backward-time evolution of initial conditions. The results in panels (c) and (d) are obtained using the Caputo derivative (2) for the forward-time (panel c) and its 'time-reversing inverse' method for the backward-time (panel d) integrations. We superimpose the forward [panels (a) and (c)] and backward [panels (b) and (d)] time evolution of three representative orbits, shown as cyan curves, with initial conditions $(x_0, y_0) = (-0.351, 0.116)$, $(x_0, y_0) = (0.525, 0.343)$, and $(x_0, y_0) = (0.186, -0.599)$, indicated by cyan points, using the respective integration methods.

The results in Fig. 4(a) and (c) are obtained using the forward Lagrangian descriptors method (7), applied to the Grünwald–Letnikov (4) and Caputo (2) derivatives, respectively. In contrast, Fig. 4(b) and (d) show the results of the backward Lagrangian descriptors method (7), computed using the 'nonlocal implicit inverse' and 'time-reversing inverse' approaches, respectively. In each panel, three cyan points indicate the initial conditions $(x_0, y_0) = (-0.351, 0.116)$, $(x_0, y_0) = (0.525, 0.343)$, and $(x_0, y_0) = (0.186, -0.599)$. Cyan curves corresponding to each initial condition are superimposed on the scalar fields and represent the time evolution of the respective orbits.

The orbits evolved forward in time [shown in Fig. 4(a) and (c) for both types of fractional derivatives] are attracted to the stable fixed points $(x, y) = (\pm 1, 0)$. Examining their backward-in-time evolution in Fig. 4(b), we observe consistent behavior: the trajectories now move away from the fixed points $(x, y) = (\pm 1, 0)$, as expected. In particular, some trajectories tend to approach the saddle point at $(x, y) = (0, 0)$ before being repelled along the unstable manifold associated with the origin. Across all three panels [Fig. 4(a), (b), and (c)], the trajectories appear to be guided by the geometric structures revealed by the Lagrangian descriptors method.

On the other hand, we observe inconsistencies in the orbital behavior shown in Fig. 4(d). Since the fixed points $(x, y) = (\pm 1, 0)$ are stable in the forward-time evolution [see Fig. 4(c)], they must act as repelling points in the backward-time integration. However, in Fig. 4(d), the cyan trajectories are also attracted to these fixed points, contradicting the expected behavior. This inconsistency indicates that the 'time-reversing inverse' method (11) is valid only for integer values of α. We, therefore, conclude that the 'nonlocal implicit inverse' method is the appropriate approach for backward-time integration in fractional-order systems, as it yields Lagrangian descriptors that accurately reflect the phase space structures of such systems.

Furthermore, this analysis explains the breaking of the infinity-shaped NHIMs observed in the first columns of Figs. 2 and 3, compared to the coherent structures seen in Fig. 1 for $\alpha = 1$. In the classical Duffing system with $\alpha = 1$, the phase space contains families of periodic orbits around the fixed points $(x, y) = (\pm 1, 0)$, enclosed by the connected stable and unstable manifolds forming the characteristic infinity-shaped structure. When fractional derivatives are introduced, the system loses the closed-loop nature of these trajectories, and for $0 < \alpha < 1$, the dynamics evolve toward stable, spiral-like behavior. As a result, the structures associated with the stable and unstable manifolds become disconnected.

5. Conclusions

In this work, we studied the behavior of a dynamical system governed by fractional-order differential equations, specifically the unforced and undamped Duffing oscillator (10), by applying the method of Lagrangian descriptors. To our knowledge, this is the first time such a method has been applied to these systems. Using different definitions of fractional derivatives and approaches for backward-in-time integration of orbits, we demonstrated that the Lagrangian descriptors method can successfully reveal the underlying geometric features that govern the system's phase space transport. We also investigated how the order α of the fractional derivatives and the integration time τ influence the morphology of the resulting phase space structures.

Our findings showed that for values of α close to the classical, integer-order Duffing oscillator ($\alpha = 1$), the phase space structures are similar to those of the classical system. However, we observed significant changes in the phase space structure as α decreases below one and τ increases. Additionally, we identified that the 'nonlocal implicit inverse' approach is the correct method for performing backward integration of fractional-order differential equations. However, it presented computational challenges for smaller values of α. Addressing the computational efficiency and accuracy of backward-in-time integration for fractional-order systems remains an important task, which we aim to tackle in the future, possibly by considering right-handed fractional derivatives as the inverse of the corresponding left-handed ones [14,81,82].

Our results highlight the effectiveness of the Lagrangian descriptors method in providing a qualitative geometric interpretation of the dynamics of systems governed by fractional-order differential equations. This method enables the exploration of phase space regions associated with distinct dynamical behaviors. We hope that this work will serve as a foundation for further applications of Lagrangian descriptors to fractional-order systems. As a natural continuation, we will report our investigation of the fractional-order Duffing oscillator with $1 < \alpha < 2$ in a future publication.

CRediT authorship contribution statement

Dylan Theron: Writing – original draft, Validation, Software, Investigation, Formal analysis, Data curation. **Hadi Susanto:** Writing – review & editing, Writing – original draft, Validation, Methodology, Conceptualization. **Makrina Agaoglou:** Writing – review & editing, Writing – original draft, Validation, Methodology, Conceptualization. **Charalampos Skokos:** Writing – review & editing, Writing – original draft, Validation, Supervision, Methodology, Conceptualization.

Declaration of competing interest

The authors declare that they have no known competing financial interests or personal relationships that could have appeared to influence the work reported in this paper.

Acknowledgments

DT acknowledges the University of Cape Town for funding assistance. HS acknowledged support by Khalifa University through a Competitive Internal Research Awards Grant (No. 8474000413/CIRA-2021-065) and Research & Innovation Grants (No. 8474000617/RIG-S-2023-031 and No. 8474000789/RIG-S-2024-070). He also acknowledges discussions with Ms. Sofwah Ahmad on fractional calculus. MA acknowledges support from the Society of Spanish Researchers in Southern Africa (ACE Sur de Africa) through the grant for the FRA Visiting Lecturers Grants Program that is sponsored by the Ramón Areces Foundation (FRA) and the Embassies of Spain in Angola, Mozambique, South Africa, and Zimbabwe. CS acknowledges support from the Research Committee (URC) of the University of Cape Town. The authors thank the High Performance Computing facility of the University of Cape Town and the Center for High Performance Computing (CHPC) of South Africa for providing computational resources for this project, and the two anonymous reviewers for their remarks and suggestions which improved the clarity of the manuscript. All authors have given their approval to the final version of the manuscript.

Data availability

Data will be made available on request.

References

[1] Ross B. The development of fractional calculus 1695–1900. Historia Math 1977;4:75–89.
[2] Kilbas AA, Srivastava HM, Trujillo JJ, editors. Theory and applications of fractional differential equations. North-Holland Mathematics Studies, 204, North-Holland; 2006.
[3] Tarasov V. Fractional dynamics: Applications of fractional calculus to dynamics of particles, fields and media. Springer Science & Business Media; 2011.
[4] Herrmann R. Fractional calculus: An introduction for physicists. World Scientific; 2011.
[5] Meral FC, Royston TJ, Magin R. Fractional calculus in viscoelasticity: An experimental study. Commun Nonlinear Sci Numer Simul 2010;15:939–45.
[6] Sasso M, Palmieri G, Amodio D. Application of fractional derivative models in linear viscoelastic problems. Mech Time-Depend Mater 2011;15:367–87.
[7] Shen L-J. Fractional derivative models for viscoelastic materials at finite deformations. Int J Solids Struct 2020;190:226–37.
[8] Bagley R, Torvik P. Fractional calculus—a different approach to the analysis of viscoelastically damped structures. AIAA J 1983;21:741–8.
[9] Agrawal OP, Baleanu D. A Hamiltonian formulation and a direct numerical scheme for fractional optimal control problems. J Vib Control 2007;13:1269–81.
[10] Tarasov V. Fractional vector calculus and fractional Maxwell's equations. Ann Physics 2008;323:2756–78.
[11] Baleanu D, Guvenc ZB, Machado JAT. New trends in nanotechnology and fractional calculus applications. Springer; 2010.
[12] Baleanu D, Diethelm K, Scalas E, Trujillo JJ. Fractional calculus: Models and numerical methods. In: Series complexity nonlineary chaos: 3, World Scientific; 2012.
[13] Atangana A, Baleanu D. New fractional derivatives with nonlocal and non-singular kernel: Theory and application to heat transfer model. Thermal Sci 2016;20:763–9.
[14] Duan J-S, Lu L, Chen L, An Y-L. Fractional model and solution for the Black–Scholes equation. Math Methods Appl Sci 2017;41:697–704.
[15] Toufik M, Atangana A. New numerical approximation of fractional derivative with non-local and non-singular kernel: Application to chaotic models. Eur Phys J Plus 2017;132:444.
[16] Sun H, Zhang Y, Baleanu D, Chen W, Chen Y. A new collection of real world applications of fractional calculus in science and engineering. Commun Nonlinear Sci Numer Simul 2018;64:213–31.
[17] Tarasov V. Handbook of fractional calculus with applications, application in physics, Part B, vol. 5, Boston: De Gruyter; 2019.
[18] Wu G-C, Shiri B, Fan Q, Feng H-R. Terminal value problems of non-homogeneous fractional linear systems with general memory kernels. J Nonlinear Math Phys 2023;30:303–14.
[19] Wu G-C, Wei J-L, Luo M. Right fractional calculus to inverse-time chaotic maps and asymptotic stability analysis. J Difference Equ Appl 2023;29:1140–55.
[20] Alfimov G, Pierantozzi T, Vázquez L. Numerical study of a fractional sine-Gordon equation. Fract. Differ. Appl 2004;4:153–62.
[21] Macías-Díaz JE. Numerical study of the process of nonlinear supratransmission in Riesz space-fractional sine-Gordon equations. Commun Nonlinear Sci Numer Simul 2017;46:89–102.

[22] Bountis T, Cantisán J, Cuevas-Maraver J, Macías-Díaz JE, Kevrekidis PG. On the fractional dynamics of kinks in Sine-Gordon models. Mathematics 2025;13:220.
[23] Podlubny I. Geometric and physical interpretation of fractional integration and fractional differentiation. Fract Calc Appl Anal 2008;5:367.
[24] Nigmatullin R. Fractional integral and its physical interpretation. Theoret and Math Phys 1992;90:242–51.
[25] Yu Z, Ren F, Zhou J. Fractional integral associated to generalized cookie-cutter set and its physical interpretation. J Phys A: Math Gen 1997;30:5569.
[26] Moshrefi-Torbati M, Hammond J. Physical and geometrical interpretation of fractional operators. J Franklin Inst 1998;335:1077–86.
[27] Cioć R. Physical and geometrical interpretation of Grünwald–Letnikov differintegrals: measurement of path and acceleration. Fract Calc Appl Anal 2016;19:161–72.
[28] Agaoglou M, Aguilar-Sanjuan B, García-Garrido V, González-Montoya F, Katsanikas M, Krajnák V, et al. Lagrangian descriptors: Discovery and quantification of phase space structure and transport. Zenodo; 2020.
[29] Daquin J, Pédenon-Orlanducci R, Agaoglou M, García-Sánchez G, Mancho A. Global dynamics visualisation from Lagrangian descriptors. applications to discrete and continuous systems. Phys D: Nonlinear Phenom 2022;442:133520.
[30] Mancho AM, Wiggins S, Curbelo J, Mendoza C. Lagrangian descriptors: A method for revealing phase space structures of general time dependent dynamical systems. Commun Nonlinear Sci Numer Simul 2013;18:3530–57.
[31] Madrid JJ, Mancho A. Distinguished trajectories in time dependent vector fields. Chaos: An Interdiscip J Nonlinear Sci 2009;19:013111.
[32] Craven GT, Hernandez R. Deconstructing field-induced ketene isomerization through Lagrangian descriptors. Phys Chem Chem Phys 2016;18:4008–18.
[33] Agaoglou M, Aguilar-Sanjuan B, García-Garrido V, García-Meseguer R, González-Montoya F, Katsanikas M, et al. Chemical reaction: A journey into phase space. Zenodo; 2019.
[34] Katsanikas M, García-Garrido V, Wiggins S. Detection of dynamical matching in a caldera Hamiltonian system using Lagrangian descriptors. Int J Bifurc Chaos 2020;30:2030026.
[35] Agaoglou M, García-Garrido V, Katsanikas M, Wiggins S. Visualizing the phase space of the HeI_2 van der Waals complex using Lagrangian descriptors. Commun Nonlinear Sci Numer Simul 2021;103:105993.
[36] Hillebrand M, Katsanikas M, Wiggins S, Skokos C. Navigating phase space transport with the origin-fate map. Phys Rev E 2023;108:024211.
[37] Revuelta F, Arranz F, Benito R, Borondo F. Unraveling the highly non linear dynamics of KCN molecular system using Lagrangian descriptors. Commun Non Linear Sci Numer Simul 2023;123:107265.
[38] Mendoza C, Mancho A. Hidden geometry of ocean flows. Phys Rev Lett 2010;105:038501.
[39] Mendoza C, Mancho A. The Lagrangian description of aperiodic flows: a case study of the Kuroshio Current. Nonlinear Process Geophys 2012;19:449–72.
[40] Smith ML, McDonald AJ. A quantitative measure of polar vortex strength using the function M. J Geophys Res Atmos 2014;119:5966–85.
[41] García-Garrido V, Ramos A, Mancho AM, Coca J, Wiggins S. A dynamical systems perspective for a real-time response to a marine oil spill. Marine Poll Bull 2016;112:201–10.
[42] Bruera R, Curbelo J, García-Sánchez G, Mancho A. Mixing and geometry in the North Atlantic Meridional overturning circulation. Geophys Res Lett 2023;50:e2022GL102244.
[43] Darwish A, Norouzi S, Di Labbio G, Kadem L. Extracting Lagrangian coherent structures in cardiovascular flows using Lagrangian descriptors. Phys Fluids 2021;33:111707.
[44] Amahjour N, García-Sánchez G, Agaoglou M, Mancho AM. Analysis of the spread of SARS-CoV-2 in a hospital isolation room using CFD and Lagrangian coherent structures. Phys D: Nonlinear Phenom 2023;453:133825.
[45] Carlo G, Montes J, Borondo F. Lagrangian descriptors for the Bunimovich stadium billiard. Phys Rev E 2022;105:014208.
[46] Hillebrand M, Zimper S, Ngapasare A, Katsanikas M, Wiggins S, Skokos C. Quantifying chaos using Lagrangian descriptors. Chaos 2022;32:123122.
[47] Zimper S, Ngapasare A, Hillebrand M, Katsanikas M, Wiggins S, Skokos C. Performance of chaos diagnostics based on Lagrangian descriptors. application to the 4D standard map. Phys D: Nonlinear Phenom 2023;453:133833.
[48] Daquin J, Charalambous C. Detection of separatrices and chaotic seas based on orbit amplitudes. Celest Mech Dyn Astron 2023;135:31.
[49] Falessi MV, Pegoraro F, Schep TJ. Lagrangian coherent structures and plasma transport processes. J Plasma Phys 2015;81:495810505.
[50] Prants S. Backward-in-time methods to simulate large-scale transport and mixing in the ocean. Phys Scr 2015;90:074054.
[51] Di Giannatale G, Falessi MV, Grasso D, Pegoraro F, Schep TJ, Veranda M, et al. Lagrangian coherent structures as a new frame to investigate the particle transport in highly chaotic magnetic systems. J Phys: Conf Ser 2018;1125:012008.
[52] Di Giannatale G, Falessi MV, Grasso D, Pegoraro F, Schep TJ. Coherent transport structures in magnetized plasmas. II. Numerical results. Phys Plasmas 2018;25:052307.
[53] Prants S. Transport barriers in geophysical flows: A review. Symmetry 2023;15:1942.
[54] Teodoro GS, Machado JT, De Oliveira EC. A review of definitions of fractional derivatives and other operators. J Comput Phys 2019;388:195–208.
[55] Li C, Zeng F. Numerical methods for fractional calculus. CRC Press; 2015.
[56] Podlubny I. Fractional differential equations: An introduction to fractional derivatives, fractional differential equations, to methods of their solution and some of their applications. Elsevier; 1998.
[57] Diethelm K. The analysis of fractional differential equations: An application-oriented exposition using differential operators of Caputo type. Berlin, Heidelberg: Springer; 2010.
[58] Scherer R, Kalla SL, Tang Y, Huang J. The Grünwald–Letnikov method for fractional differential equations. Comput Math Appl 2011;62:902–17.
[59] Lopesino C, Balibrea F, Garcia-Garrido V, Wiggins S, Mancho A. A theoretical framework for Lagrangian descriptors. Int J Bifurc Chaos 2017;27:1730001.
[60] Eldering J. Normally hyperbolic invariant manifolds: The noncompact case. Springer; 2013.
[61] Demian A, Wiggins S. Detection of periodic orbits in Hamiltonian systems using Lagrangian descriptors. Int J Bifurc Chaos 2017;27:1750225.
[62] Katsanikas M, García-Garrido V, Agaoglou M, Wiggins S. Phase space analysis of the dynamics on a potential energy surface with an entrance channel and two potential wells. Phys Rev E 2020;102:012215.
[63] Lopesino C, Balibrea F, Wiggins S, Mancho A. Lagrangian descriptors for two dimensional, area preserving, autonomous and nonautonomous maps. Commun Nonlinear Sci Numer Simul 2015;27:40–51.
[64] Duffing G. Erzwungene Schwingungen bei veränderlicher Eigenfrequenz und ihre technische Bedeutung. Friedrich Vieweg & Sohn; 1918.
[65] Li Z, Chen D, Zhu J, Liu Y. Nonlinear dynamics of fractional order Duffing system. Chaos Solitons Fractals 2015;81:111–6.
[66] Ilhan E. Interesting and complex behaviour of Duffing equations within the frame of Caputo fractional operator. Phys Scr 2022;97:054005.
[67] Li X, Wang Y, Shen Y. Cluster oscillation of a fractional-order Duffing system with slow variable parameter excitation. Fractal Fract 2022;6:295.
[68] Jiménez S, González J, Vázquez L. Fractional Duffing's equation and geometrical resonance. Int J Bifurc Chaos 2013;23:1350089.
[69] Xu Y, Li Y, Liu D, Jia W, Huang H. Responses of Duffing oscillator with fractional damping and random phase. Nonlinear Dynam 2013;74:745–53.
[70] Jiménez S, Zufiria PJ. Characterizing chaos in a type of fractional Duffing's equation. Dyn Syst Differ Equ Appl AIMS Proc 2015;660–9.
[71] Torkzadeh L. Numerical behavior of nonlinear Duffing equations with fractional damping. Rom Rep Phys 2021;73:113.
[72] Rysak A, Sedlmayr M. Damping efficiency of the Duffing system with additional fractional terms. Appl Math Model 2022;111:521–33.
[73] Hamaizia S, Jiménez S, Velasco MP. Rich phenomenology of the solutions in a fractional Duffing equation. Fract Calc Appl Anal 2024;27:1017–47.
[74] Balibrea-Iniesta F, Lopesino C, Wiggins S, Mancho A. Lagrangian descriptors for stochastic differential equations: A tool for revealing the phase portrait of stochastic dynamical systems. Int J Bifurc Chaos 2016;26:1630036.
[75] Campos RG. Time-reversal breaking in fractional differential problems. Eur Phys J Plus 2015;130:1–5.

[76] Li Y, Zhao D, Chen Y, Podlubny I, Zhang C. Finite energy Lyapunov function candidate for fractional order general nonlinear systems. Commun Nonlinear Sci Numer Simul 2019;78:104886.
[77] Matignon D. Stability results for fractional differential equations with applications to control processing. In: Computational engineering in systems applications, vol. 2, Lille, France; 1996, p. 963–8.
[78] Cong ND, Doan T, Siegmund S, Tuan H. An instability theorem for nonlinear fractional differential systems. Discret Contin Dyn Syst - B 2017;22:3079–90.
[79] Cong ND, Doan TS, Siegmund S, Tuan H. Linearized asymptotic stability for fractional differential equations. Electron J Qual Theory Differ Equ 2016;39:1–13.
[80] Qian D, Li C, Agarwal RP, Wong PJ. Stability analysis of fractional differential system with Riemann–Liouville derivative. Math Comput Modelling 2010;52:862–74.
[81] Wu G-C, Wei J-L, Luo M. Right fractional calculus to inverse-time chaotic maps and asymptotic stability analysis. J Difference Equ Appl 2023;29:1140–55.
[82] Wu G-C, Shiri B, Fan Q, Feng H-R. Terminal value problems of non-homogeneous fractional linear systems with general memory kernels. J Nonlinear Math Phys 2023;30:303–14.